Influence of Spectral Bandwidth on the Working Curve in Vat Photopolymerization*

Benjamin W. Caplins[a,*], Thomas J. Kolibaba[a], Uwe Arp[b], C. Cameron Miller[b], Yuqin Zong[b], Dianne L. Poster[b], Callie I. Higgins[a], Jason P. Killgore[a]

[a] *National Institute of Standards and Technology, 325 Broadway, Boulder, CO, 80305, United States*
[b] *National Institute of Standards and Technology, 100 Bureau Drive, Gaithersburg, MD, 20899, United States*

Abstract

In vat photopolymerization, 3-dimensional parts are fabricated by using patterned light to spatially cure a liquid resin. One of the foundational measurements for vat photopolymerization is known as the *working curve* whereby the depth (*i.e.* thickness) of cured resin is measured as a function of radiant exposure. The commonly applied mathematical model for the working curve – known widely as the *Jacobs model* – assumes a monochromatic light source. The Jacobs model has been widely used, but in many cases significant deviations between the Jacobs model and the data have been observed. Herein, we extend the Jacobs model by deriving a polychromatic model that accounts for broadband light sources (*e.g.* light emitting diodes, LEDs). We demonstrate through experiment and theory that in certain cases the deviations from Jacobs' original model can be explained and understood as an optical 'inner filter' effect. The ability of the Jacobs model to capture the working curve behavior is shown to be dependent on the bandwidth of the light source in conjunction with the gradient in the absorption spectrum of the resin in the vicinity of the light source spectrum. Additionally, we offer an empirical model function that better fits experimental data and allows for an improved estimate of model parameters. Broadly, this work aims to strengthen the conceptual link between the working curve measurement and the photophysical parameters that are intrinsic to vat photopolymerization printing.

Keywords: Digital Light Processing (DLP), Vat Photopolymerization, Masked Stereolithography (MSLA), Light Emitting Diode (LED), Working Curve

1. Introduction

Vat photopolymerization (VP) is an additive manufacturing technique where a liquid resin is cured into a solid polymer by means of spatially patterned light to generate a 3-dimensional part with an arbitrary geometry. The modern version of the technique was developed in the 1980's[1, 2] and since that time has grown rapidly in numerous market sectors including dental, automotive, and medical markets. The process of VP printing involves a complex interplay of different physical processes[3, 4, 5, 6] (chemical kinetics, heat, optics, diffusion, etc) and a complete model for the process of forming solid parts is not readily available. Even though there is no complete model available, simple models exist that have either explanatory or even predictive power for one or a few variables at a time.

Some of the best-known mathematical relationships in VP were described in a 1992 publication by Jacobs entitled *Fundamentals of Stereolithography*[7]. One of the most enduring concepts from that work is known

*Contribution of NIST, an agency of the US government; not subject to copyright in the United States.
**Commercial equipment, instruments, or materials are identified only in order to adequately specify certain procedures. In no case does such identification imply recommendation or endorsement by the National Institute of Standards and technology, nor does it imply that the products identified are necessarily the best available for the purpose.

*Corresponding Author
Email address: benjamin.caplins@nist.gov (Benjamin W. Caplins)

as the *working curve* which relates the radiant exposure[1] at the surface of the photopolymer resin to the thickness of cured polymer. Jacobs developed a simple model for the working curve which is often used,

$$C_d(E_0) = D_p \ln\left(\frac{E_0}{E_c}\right). \tag{1}$$

Here, C_d is the depth (*i.e.* thickness) of cured polymer (units of length), D_p is the optical penetration depth of the light source into the resin (units of length), E_0 is the radiant exposure (units of energy per unit area), and E_c is the minimal radiant exposure necessary to transform (*i.e.* cure) the liquid resin into a solid (units of energy per unit area). Jacobs described Eq. 1 as being "absolutely fundamental to an understanding of this technology"[7] and it has been widely utilized by both industry and academia to model the photopolymerization process. As a point of nomenclature, we denote the *working curve* as a graph of data relating the cure depth to the incident radiant exposure (typically plotted on a logarithmic exposure axis), and Eq. 1 is referred to as the *Jacobs model* that can be fit to the working curve data using a least squares method by leaving D_p and E_c as free parameters. In the Jacobs model, it is implicit that D_p can be obtained from optical absorption measurements of the resin, though the validity of this has only occasionally been explored[9]. The Jacobs model fit can then either be used to extrapolate/interpolate the cure depth for any radiant exposure in print parameter optimization, or the D_p and E_c parameters can be used to understand printability of a resin formulation. For example, printing with high spatial resolution is thought to be best achieved when D_p is on the same order of magnitude as the desired resolution. Similarly, higher print speed is best achieved with more reactive (*i.e.* lower E_c) resins.

Despite the widespread use of the Jacobs model to describe experimentally measured working curves, there are frequently notable systematic deviations from the model (*e.g.* Refs. [10, 11, 12]). Most of the time, these deviations are explained by assuming that the optical properties of the resin are changing in real-time serving to make the D_p a function of radiant exposure, E_0. Thus, the optical properties implicitly depend on the duration of the exposure and the depth at which those properties are measured. In this context, a exposure-dependent D_p manifests as nonlinear behavior of the working curve when plotted with a logarithmic exposure axis. The most common causes invoked for changing optical properties are either photobleaching[13, 14, 15, 16, 17, 18] or a difference in the absorption coefficient between the liquid and solid[19, 20]. One other cause for deviations from the Jacobs model is due to the polychromatic or broadband nature of commonly used light sources. Gong *et al.*[9] followed by van der Linden *et al.*[21] found that the bandwidth of light emitting diode (LED) sources can be sufficient to give rise to what can be termed an 'inner filter effect'[22] whereby the resin absorption acts to shift the spectrum of the light as a function of depth. This depth-dependent light spectrum then causes a depth-dependent (and thus exposure- and time-dependent) D_p. These authors emphasized that modern LED sources are broadband relative to laser-based sources and photopolymer curing models need to consider the interaction of the polychromatic light source with the resin to achieve reasonable agreement with experiment[9, 21].

[1] Historically, the term 'dose' was used instead of 'radiant exposure' to describe the area normalized amount of optical energy incident on the sample, however, 'dose' is not consistent with the SI unit system[8]. Thus, herein we use 'radiant exposure' or simply 'exposure' to refer to the area normalized optical energy incident on the photopolymer resin.

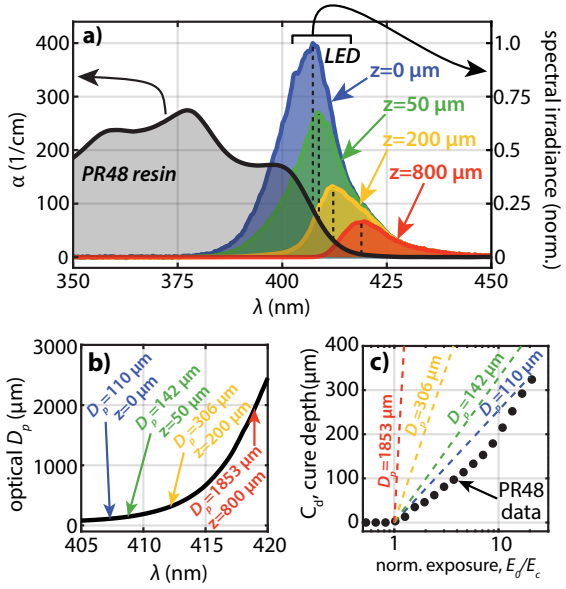

Figure 1: Depiction of the inner filter effect for the PR48 resin. (a) The absorption coefficient of PR48 is shown alongside the LED spectrum calculated (with using Beer's law) at different depths as it propagates through the resin. These data were collected in our laboratory. (b) The plot of the optical D_p ($D_p = 1/\alpha$) as a function of wavelength noting the D_p for several different propagation depths. (c) A working curve for PR48 plotted on a normalized exposure axis overlaid with several Jacobs models using the D_p's noted in (b). Data are plotted with a logarithmic exposure axis.

As an example, the inner filter effect is depicted in Fig. 1 for a commonly used printing wavelength (405 nm) with a widely studied open-source photopolymer resin (CPS, PR48). In Fig. 1a the absorption coefficient, $\alpha = 1/D_p$ [9], of PR48 is shown alongside to a LED spectrum at different depths as it propagates through the resin. Here, the LED spectrum was directly measured at $z = 0$ and for $z > 0$ Beer's law was used to calculate the spectra. The $\lambda_{\max}$ red shifts as a function of depth and this is noted in Fig. 1b on a plot of the optical $D_p(\lambda)$. Fig. 1c shows example working curve data obtained with the Jacobs model predictions for the values of D_p corresponding to different $\lambda_{\max}$. Thus, *as the light source spectrum propagates through the resin, the spectrum shifts towards lower α which has the effect of steepening the working curve as the exposure is increased.* The changing slope (on a logarithmic exposure axis) is a clear deviation from the Jacobs model. This effect is expected to be negligible for narrow band (monochromatic) sources.

Herein we extend the work of Jacobs by incorporating the ideas from Gong *et al.*[9] and van der Linden *et al.*[21] by developing a polychromatic model for the working curve. We demonstrate the validity of this model by formulating resins with different optical properties and performing measurements of their working curves with both narrowband and broadband illumination. We show that the polychromatic model predicts the deviations from the Jacobs model for these resins without the need to rely heavily on other explanations.

2. Theoretical Models

In this manuscript we discuss three distinct mathematical models. To begin, we derive the *Jacobs model* with an emphasis on the assumptions implicit to the model – in the context of this work, the most important of which is the assumption of a monochromatic light source. Then we extend the Jacobs model to account for polychromatic light sources, which we denote the *polychromatic model* for the working curve. Finally, we present an empirical model – denoted the *delta model* – for the working curve that fits experimental data well and simplifies to the Jacobs model in ideal circumstances.

2.1. Jacobs Model

We begin with a few assumptions from which the Jacobs model follows:

- The illumination is uniform in the xy plane such that only the z direction must be considered.
- The resin is a homogeneous solution where the only optically active species are photoinitiator and photoblocker. This allows us to write, $\alpha^{\Sigma}_{\lambda_0} = \alpha^{PI}_{\lambda_0} + \alpha^{PB}_{\lambda_0}$ where $\alpha^{\Sigma}_{\lambda_0}$ is the base-e absorption coefficient (units of inverse length) of the total resin, which is the sum of the absorption coefficients of the photoinitiator and photoblocker species. All absorption coefficients are given at the wavelength of the light source, λ_0. The light source is assumed to be monochromatic.
- The propagation of light through the resin conforms to Beer's law. Hence, the radiant exposure profile, $E(z,t)$, is given by a simple exponential function,

$$E(z,t) = E_0(t)\exp(-\alpha^{\Sigma}_{\lambda_0} z) \tag{2}$$

  where $E_0(t) = tI_0$ expresses the total incident radiant exposure, $E_0(t)$, (units of energy per unit area) as a function of the incident irradiance, I_0, (units of energy per unit area per unit time) and the exposure duration, t (units of time). Here it is assumed that the exposure reciprocity law is obeyed such that only the exposure need be considered[23]:

$$E(z,E_0) = E_0\exp(-\alpha^{\Sigma}_{\lambda_0} z). \tag{3}$$

- The resin changes from a liquid to a solid when a certain density of photoinitiation events have occurred. Here, we use energy density as a proxy for the photoinitiation event density. To write the energy density absorbed by the photoinitator, $A^{PI}(z,E_0)$ (energy per unit volume), we multiply the exposure by the absorption coefficient of the photoinitator species,

$$A^{PI}(z,E_0) = \alpha^{PI}_{\lambda_0} E_0\exp(-\alpha^{\Sigma}_{\lambda_0} z) \tag{4}$$

  and thus we assume that when $A^{PI}(z,E_0) = A^{PI}_{crit}$ the resin is cured to a depth $z = C_d$,

$$A^{PI}_{crit} = \alpha^{PI}_{\lambda_0} E_0\exp(-\alpha^{\Sigma}_{\lambda_0} C_d). \tag{5}$$

To recover the Jacobs model from these assumptions we solve Eq. 5 for C_d,

$$C_d(E_0) = \frac{1}{\alpha^{\Sigma}_{\lambda}}\ln\left(\frac{E_0}{A^{PI}_{crit}/\alpha^{PI}_{\lambda}}\right). \tag{6}$$

and we identify $D_p = 1/\alpha^{\Sigma}_{\lambda}$ and $E_c = A^{PI}_{crit}/\alpha^{PI}_{\lambda}$ to yield the exact result of Jacobs (leaving the time-dependence of E_0 implicit),

$$C_d(E_0) = D_p\ln\left(\frac{E_0}{E_c}\right). \tag{7}$$

An important point to note here is that *even in this extremely simple model, D_p and E_c are functions of wavelength* through the fact that the absorption coefficients are functions of wavelength. For context, when the Jacobs model was derived, laser illumination was assumed and so the assumption of a fixed wavelength monochromatic source was quite sensible.

2.2. Polychromatic Model

In the Jacobs model derived in the previous section, the light source was assumed to be monochromatic. For polychromatic light we introduce a lineshape function, $S(\lambda)$ (units of inverse wavelength), which is unit normalized,

$$\int_0^{\infty} S(\lambda)\, d\lambda = 1. \tag{8}$$

This permits us to write the spectrally resolved exposure profile (energy per unit time per unit area per unit wavelength) as,

$$E(z, E_0, \lambda) = E_0 S(\lambda) \exp(-\alpha^{\Sigma}(\lambda) z). \tag{9}$$

Similar to the Jacobs model derivation, we next calculate the energy density absorbed by the photoinitator and assume that a critical energy density absorbed by the photoinitiator will cause the photopolymer to solidify. The only differences are that we must integrate over the source spectrum and the wavelength dependence of the absorption coefficient is now made explicit,

$$A^{PI}_{crit} = E_0 \int_0^{\infty} \alpha^{PI}(\lambda) S(\lambda) \exp(-\alpha^{\Sigma}(\lambda) C_d)\, d\lambda. \tag{10}$$

In contrast to the Jacobs model, C_d cannot be easily expressed as a function of E_0. Instead, we can express E_0 as a function of C_d (leaving the time-dependence implicit),

$$E_0(C_d) = \frac{A^{PI}_{crit}}{\int_0^{\infty} \alpha^{PI}(\lambda) S(\lambda) \exp(-\alpha^{\Sigma}(\lambda) C_d)\, d\lambda}. \tag{11}$$

Finally, we can rewrite the equation in terms of the more familiar E_c instead of A^{PI}_{crit} by noting that,

$$E_c = \lim_{C_d \to 0} E_0(C_d) = \frac{A^{PI}_{crit}}{\int_0^{\infty} \alpha^{PI}(\lambda) S(\lambda)\, d\lambda}. \tag{12}$$

Combining Eqs. 11 and 12 we finally have a full expression for what we call the *polychromatic model* for the working curve,

$$\frac{E_0(C_d)}{E_c} = \frac{\int_0^{\infty} \alpha^{PI}(\lambda) S(\lambda)\, d\lambda}{\int_0^{\infty} \alpha^{PI}(\lambda) S(\lambda) \exp(-\alpha^{\Sigma}(\lambda) C_d)\, d\lambda}. \tag{13}$$

Here $S(\lambda)$, $\alpha^{PI}(\lambda)$, and $\alpha^{\Sigma}(\lambda)$ can all be experimentally measured. Specifically, $S(\lambda)$ can be measured with a properly calibrated spectrometer and $\alpha^{PI}(\lambda)$ and $\alpha^{\Sigma}(\lambda)$ are given by the UV/Vis absorption spectrum before and after the photoblocker is added, respectively. Thus, with these measurements in hand, Eq. 13 can be numerically integrated for a range of C_d values to generate a plot of C_d vs E_0 with only a single unknown parameter, E_c. This result is conceptually identical to that of the Jacobs model where E_c is unknown and D_p is theoretically given by the absorption spectrum. The polychromatic model (Eq. 13) differs from the basic result of Gong *et al.*[9] with the inclusion of the photoinitiator absorption coefficient term.

2.3. Delta Model

Finally, we present an empirical model that we have found to fit a wider range of experimental working curve data than the Jacobs model,

$$C_d(E_0) = \left[\frac{1 + \delta \frac{E_0}{E_c}}{1 + \delta}\right] \times D_p \ln\left(\frac{E_0}{E_c}\right). \tag{14}$$

This model is referred to as the *delta model* and it has one extra parameter, δ, compared to the Jacobs model. It was defined such that when $\delta = 0$ the first term (in square brackets) reduces to 1 and we recover the Jacobs model exactly. Additionally, the derivative of the delta model (*i.e.*, $\frac{\mathrm{d}C_d}{\mathrm{d}\ln(E_0)}$) matches that of the Jacobs model at $E_0 = E_c$ when the models have the same D_p parameter. While the physical meaning of the δ parameter is not well-defined at present, the ability of the delta model to fit experimental data and allow for the extraction of more accurate D_p and E_c parameters is of practical utility.

3. Methods

3.1. Materials

The multifunctional crosslinkers SR494 and PRO13514 were provided by Sartomer (Exton, PA, USA). The reactive diluent Genomer 1122 was provided by Rahn USA (Aurora, IL, USA). The photoinitiator diphenyl(2,4,6-trimethylbenzoyl)phosphine oxide (TPO, 97%) and photoabsorbers 2,5-Bis(5-tert-butylbenzoxazol-2-yl)thiophene (BBOT, 99%) and 1-phenylazo-2-naphthol (Sudan I, > 95%) were purchased from Sigma Aldrich (St. Louis, MO, USA). All chemicals were used without further purification.

3.2. Resin Formulation

A mixture of the polymerizable components SR494 (40 % by mass), PRO13514 (40 % by mass), and Genomer 1122 (20 % by mass) were prepared in an amber bottle and stirred overnight to homogeneity. Aliquots of this mixture were used to prepare three photopolymerizable resins containing optically active ingredients: TPO; TPO and BBOT; TPO and Sudan I. The final concentration of TPO for all resins was 0.4 % (by mass). The final concentrations of BBOT and Sudan I resins were 0.16 % (by mass) and 0.14 % (by mass), respectively. These concentrations were chose to yield photopolymerization resins comparable to the commercially available PR48 resin. Photopolymerizable resins were prepared in scintillation vials and vortexed (VWR, MiniVortexer) for 1 minute at max intensity and then placed in a ultrasonic bath (VWR, Symphony) without additional heat for one hour then allowed to sit unperturbed overnight prior to analysis or further use. Samples were stored in an amber jar between preparation and analysis.

3.3. UV/Vis Measurements

UV/Vis absorption measurements were collected for each resin configuration from 350 nm to 700 nm using a quartz 100 µm pathlength demountable cuvette (Starna Cells, 20/C-Q-0.1) on a commercial spectrometer (Thermo Scientific, Evolution 60S) with 0.5 nm step size. Isopropyl alcohol was used for blanking the spectrometer. Repeated measurements evidenced small shifts in the baseline (*i.e.* imperfect referencing) and these shifts were removed by subtracting a linear background fit to the data > 50 nm to longer wavelengths of the main absorption edge. Note that all absorption coefficients in this manuscript are base-e and not base-10.

3.4. LED Spectral Irradiance Measurement

To obtain the spectrally resolved lineshape measurement of the LED source a fiber coupled spectrometer (Avantes, AvaSpec-ULS4096CL-EVO) was used that has 1 nm spectral resolution. The wavelength calibration was verified using a Hg/Ar lamp. A cosine corrector (Thorlabs, CCSA1) was used as the sampling optic to limit sensitivity to the optical alignment/angle of incidence. The instrument response function of the fiber optic and spectrometer was measured using a NIST traceable halogen light source. The spectral transmission of the cosine corrector optic was provided by the manufacturer and was numerically incorporated into the instrument response function. Spectra were dark count subtracted and divided by the instrument response function to ensure the spectral lineshapes were expressed in terms of the relative spectral irradiance.

3.5. Working Curve Measurement

A schematic of the working curve measurement is shown in Fig. 2a. The light engine for the working curve exposures consisted of multichannel current driver (Vektrex, SS400-PRF-100-5-2U8) driving a hexagonal array of LEDs (Luminus, SBM-120-UV-R34) that are mounted on a thermoelectric baseplate (Arroyo, 5400-15-28/274) as shown in Fig. 2b. The baseplate for the LEDs was maintained at 25 °C during experiments. The light source was placed 150 mm below the sample plane and results in a light cone half-angle of *ca.* 10°. A 1.1 mm thick piece of Gorilla glass (Edmund Optics, 11-855) was used as a working surface to ensure resin did not drip onto the light source. To achieve an irradiance of 10 mW/cm^2 with no spectral filtering of the LED output (*i.e.* broadband illumination), three LEDs were each driven with 0.32 A of current. To achieve an irradiance of 10 mW/cm^2 with a narrow bandpass filter (Semrock, LL01-405-12.5) inserted before the sample plane (*i.e.* narrowband illumination), six LEDs were each driven with 1.6 A of current. The

steady state optical power was determined by measuring the power transmitted through a 2 mm diameter aperture using a silicon-based power meter set to measure 405 nm light (Thorlabs, PM100D/S120VC). Due to the pulsed nature of the experiments and despite the temperature controlled baseplate, the LED junction temperature changes during the experiment which affects the light output and wavelength, however, this effect was negligible for the purposes of this study. No index matching fluids were used in the system and so Fresnel reflections are present in the system, but this should not impact the conclusions of this work because they would be present in all experiments uniformly.

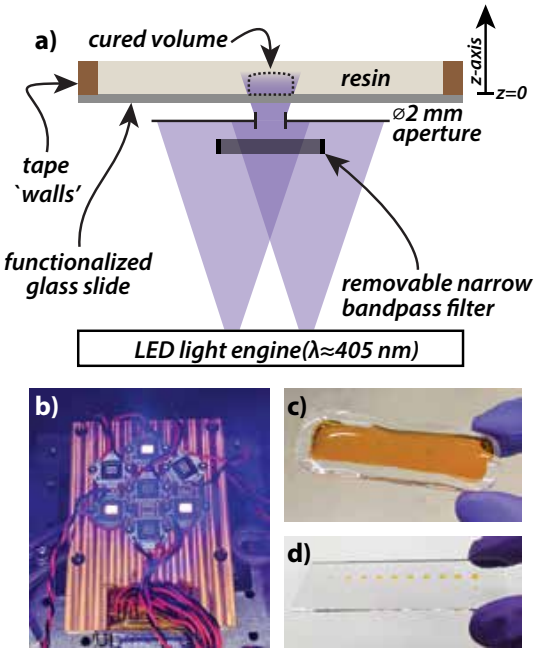

Figure 2: (a) A schematic of the working curve experiment. An LED light engine exposes a resin through a 2 mm diameter aperture. The resin is contained on a methacrylate-functionalized glass slide. The spectrum can be modified to be narrowband via the addition of a narrow bandpass filter. The Gorilla glass is located below the bandpass filter and is not shown. (b) The actual light source with three LED's turned on. (c) The glass slide with tape walls loaded with resin ready for a working curve measurement. (d) The result of the working curve measurement after rinsing and post-curing.

The photopolymer resins were placed on glass slides (25 mm × 75 mm × 1 mm) surface-functionalized with 3-(trimethoxysilyl) propyl methacrylate (PolyAn, Berlin, Germany) to improve adhesion of the cured resin to the substrate. A removable tape was applied at the edges of the slide to contain the resin and allow for a > 2 mm deep volume of resin which ensured that the cure depths were significantly less (in this case, the max cure depth was < 500 µm) than the resin depth (Fig. 2c). The area for each exposure was defined by a 2 mm diameter aperture placed directly beneath the slide. Exposures were performed in a 2 × 10 grid leaving 4 mm between successive exposures. Following a set of exposures, the slide was immediately rinsed with copious amounts of isopropyl alcohol, dried under a stream of air, and post-cured in a light box (Asiga, Flash) for 180 s. Height measurements on the post-cured slide (Fig. 2d) were performed on a low force micrometer (Mitutoyo, VL-50A).

4. Results

4.1. Working Curves in Custom Resins

The polychromatic model for the working curve given in Eq. 13 requires knowledge of the optical properties of the resin in addition to the spectral output of the light source. Herein, we systematically vary both

the resin and the light source to verify the applicability of the polychromatic model. The model specifically requires the absorption of the resin with and without any photoblocker present as input parameters. In Fig. 3a the absorption coefficient for the resin lacking photoblocker is given ($\times 10$) in addition to the absorption coefficient for resins containing two different photoblockers. The resin with BBOT photoblocker yields a resin similar to PR48 that is optically clear to the human eye and has an absorption edge at *ca.* 410 nm. The resin with Sudan I photoblocker yields a resin that is orange in appearance with an absorption edge at *ca.* 530 nm. The absorption curves of the photoblocker-containing resins intersect at 407 nm and so from the perspective of the Jacobs model, it might be assumed that the working curves measured with a 405 nm light source would appear similar. Importantly, the gradients near 405 nm in the absorption curves are quite different between the two resins, with the BBOT resin having a steep gradient and the Sudan I resin having a plateau. Thus, from the perspective of the polychromatic model for the working curve, these resins might be expected to have notably different behaviors. Or phrased slightly differently, the variation of optical parameters across the bandwidth of the broadband source is minimal for the Sudan I resin, and notable for the BBOT resin, while the variation of the optical parameters across the bandwidth of the narrowband source is negligible.

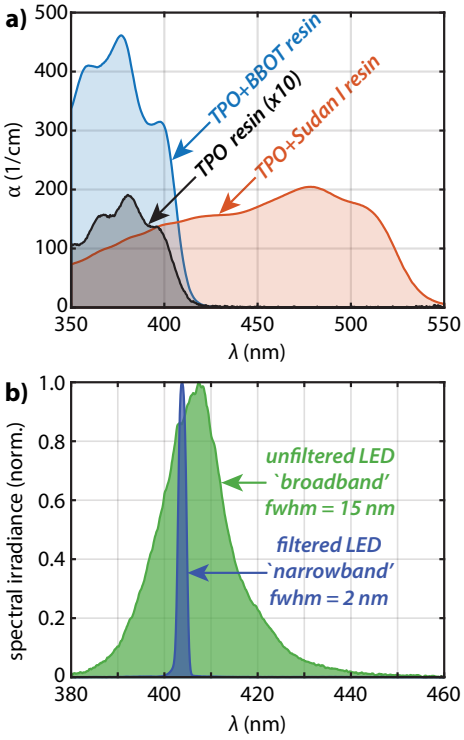

Figure 3: (a) The measured absorption coefficients necessary for the calculation of the polychromatic model. Note that the TPO-only resin (*i.e.* only photoinitiator and no photoblocker) is scaled by $\times 10$ for viewing. (b) The measured spectrum of the LED light engine with and without a narrow bandpass filter.

Working curves of these resins were obtained using broadband and narrowband illumination – the narrowband light was obtained by spectrally filtering the native LED output with a bandpass filter. The light source spectra are shown in Fig. 3b. The broadband spectrum has a 15 nm full width at half maximum (fwhm) while the narrowband spectrum has a 2 nm fwhm.

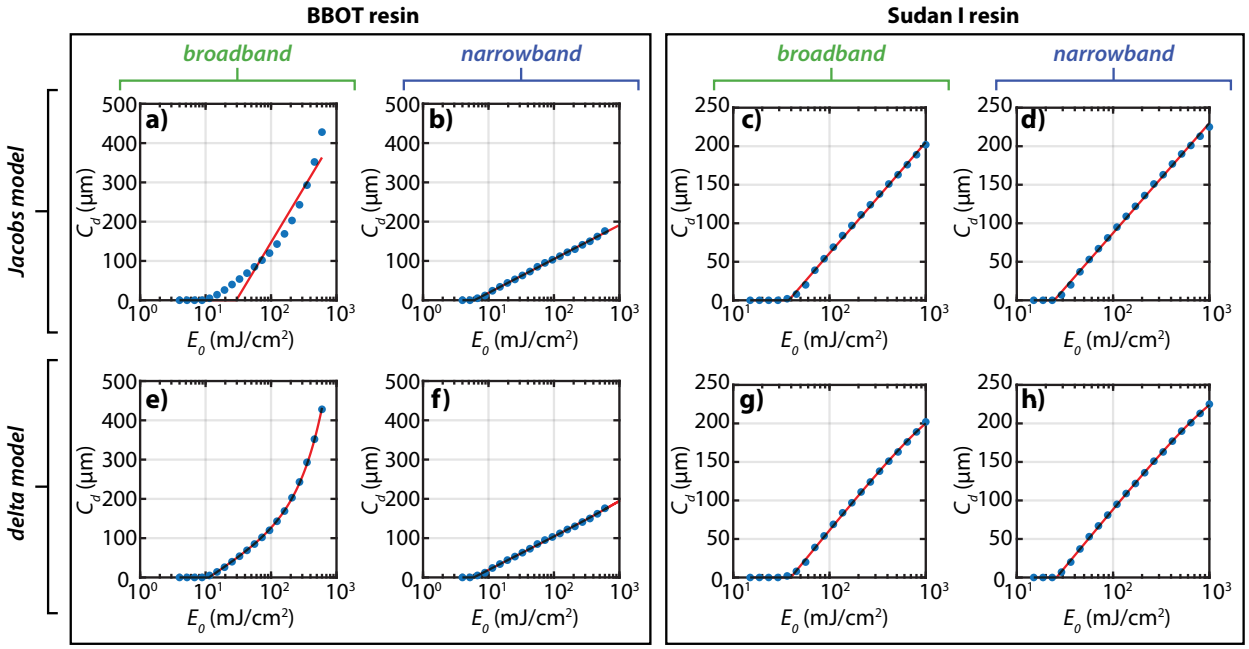

Figure 4: (a-d) Raw working curve data overlaid with the best-fit to the Jacobs model. (e-h) The same data as (a-d) except fit to the delta model. Note the poor agreement between the Jacobs model and the working curve of the BBOT resin obtained with broadband illumination. A typical explanation of this deviation from the Jacobs model would involved photobleaching of the resin, however, the working curve of the same resin collected with narrowband illumination fits well to the Jacobs model and seems to rule out this explanation. All data are plotted with a logarithmic exposure axis.

Working curves were measured on the BBOT-based resin in addition to the Sudan I-based resin using both the narrowband and broadband illumination. In Fig. 4a-d the raw data for these working curves are shown with least squares fits to the Jacobs model (Eq. 1) and in Fig. 4e-h the same data are shown fit to the delta model (Eq. 14). Using broadband illumination with the BBOT photoblocker yields a working curve that strongly deviates from the Jacobs model fit while using narrowband illumination yields a working curve that is well-fit by the Jacobs model. Since all of these experiments have nominally the same irradiance and are centered close to the same wavelength, this rules out photobleaching as being the dominant cause for the upwards curvature of the data (when plotted on a logarithmic exposure axis). In contrast to the BBOT data, the data for the Sudan I-based resin is well-fit to the Jacobs model for both narrowband and broadband light sources. This further suggests that photobleaching makes a minimal contribution to the shape of the working curve in these systems.

Using the delta model to fit the working curve data (Fig. 4e-h) results in high quality fits for all datasets. The delta model fit to the polychromatic working curve on the BBOT resin has a δ parameter significantly greater than zero, which is able to account for the curvature of the data significantly better than the Jacobs model. While the δ parameter cannot currently be given a physical interpretation, when it deviates from zero in a statistically significant manner it indicates that the Jacobs model is inapplicable to the data. It is likely that the δ parameter will increase monotonically with both the light source bandwidth and the gradient in the absorption spectrum. From a practical perspective, the delta model tracks the data well and can be used to estimate the D_p (in the limit of zero cure depth) and the E_c value with improved fidelity relative to the Jacobs model. The extraction of these parameters (regardless of the interpretability of the δ parameter) allows the data to be plotted in normalized units (*e.g.* C_d/D_p and/or E_0/E_c) which permits for a more general comparison of datasets (see below).

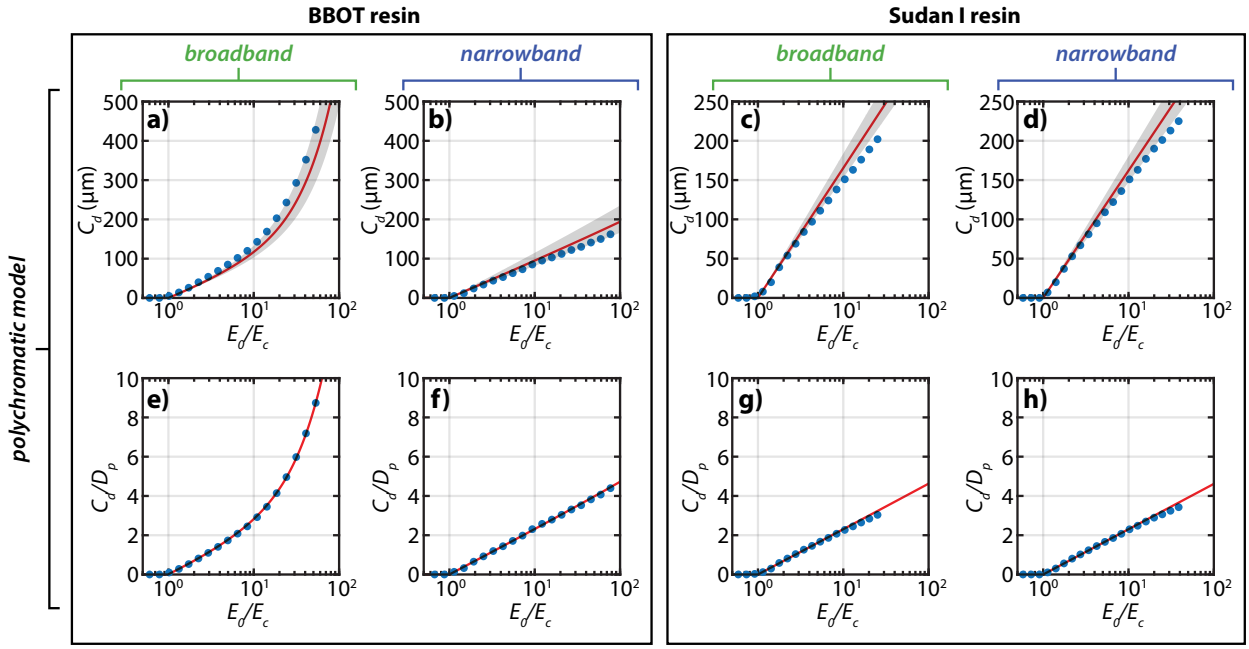

Figure 5: (a-d) The same working curve data as in Fig. 4a-d except plotted on a normalized exposure axis and overlaid with the predictions from the polychromatic model. The grey shaded region corresponds to an estimate of the uncertainty associated with the measurement of the optical parameters that are used in polychromatic model calculation. (e-h) The same data as in (a-d) exception plotted on doubly normalized axes and without the uncertainty estimate. Here the vertical axis for the polychromatic model and the experimental data are normalized independently. The polychromatic model is able to capture the deviation of the working curve data from the Jacobs model for the the BBOT resin/broadband illumination experiment. For reference, on doubly normalized axes all Jacobs models appear identical. All data are plotted with a logarithmic exposure axis.

The polychromatic model for the working curve is unable to predict the E_c parameter and so to compare the data to the model we plot the data on a normalized exposure axis using the delta model to estimate E_c for the data. *On this normalized exposure axis, the polychromatic model has no free parameters.* The model predictions and data are plotted in Fig. 5a-d with a grey shaded region giving an estimate of the uncertainty in the model due to the optical measurements that are input into the model. Specifically, the polychromatic model was calculated allowing for a ±1 nm shift in the absorption spectra relative to the light source spectrum in addition to allowing for a 10 % variation in the absorbance measurements. While not a rigorous error analysis, these types of variations are experimentally reasonable and give an idea of how sensitive the model is to the optical parameters. In all cases, the polychromatic model is in qualitative agreement with the data and is nearly in quantitative agreement. The model captures the curvature of the broadband light source with the BBOT-based resin and also captures the lack of curvature in the other three cases. This is strong evidence that the deviation from the Jacobs model for the BBOT-based resin is due to the variation of resin optical properties that exist across the bandwidth of the LED light source and rules out the need to invoke photobleaching to explain the discrepancy.

As a final check, we plot the polychromatic model overlaid with the experimental data on doubly normalized axes (E_0/E_c and C_d/D_p, using the delta model parameters to normalize the data). Plotting the data in this manner (Fig. 5e-h) ensures that the experiments were conducted over a sufficient range of exposures and cure depths to make meaningful comparisons. This presentation of the data removes two degrees of freedom from the data and emphasizes the agreement in the curvature (on a logarithmic exposure axis) predicted by the model. In all cases, the model is consistent with the data. Note that all of the model fit parameters used for normalization are given in the Appendix (Table A.1).

5. Working Curves in Commercial Resins

The custom resins developed for these studies show the importance and validity of the polychromatic model to be applied to the working curve. These resins are based on the PR48 resin formulation and are not necessarily representative of all resins. Thus, we selected three 'clear' (*i.e.*, appear clear to the human eye) commercial resins and collected working curve data with narrow and broadband illumination. Note that we cannot calculate the polychromatic model for these resins since we do not know the formulation and thus cannot determine $\alpha^{PI}(\lambda)$, though the absorption coefficient for the resins is shown in Fig. 6a. These working curve data were fit to the delta model (fits not shown, fit parameters are given in the Appendix, Table A.1) to extract the E_c and D_p parameters and plotted in doubly normalized units in Fig. 6b-d. Again, we plot the data in these normalized units to ensure that the measurements were performed over a sufficient range of exposures and cure depths. For the commercial resin 'A' there was little difference between the two light sources and minimal deviation from the linear (*i.e.*, Jacobs model) behavior. In contrast, for commercial resins 'B' and 'C' there is qualitatively different behavior between the working curve data collected with narrowband and broadband illumination in addition to a significant departure from the Jacobs model. Typically, a departure from the Jacobs model is assigned to photobleaching or changes to the optical properties of the resin upon curing. However, these data are not easily explained by those mechanisms since only the light source bandwidth changes in these experiments and thus a comparable degree of photobleaching would be expected in both experiments. Thus, we speculate that the major cause for deviation from the Jacobs model is due to the polychromatic nature of the LED light source and how that propagates through the resin.

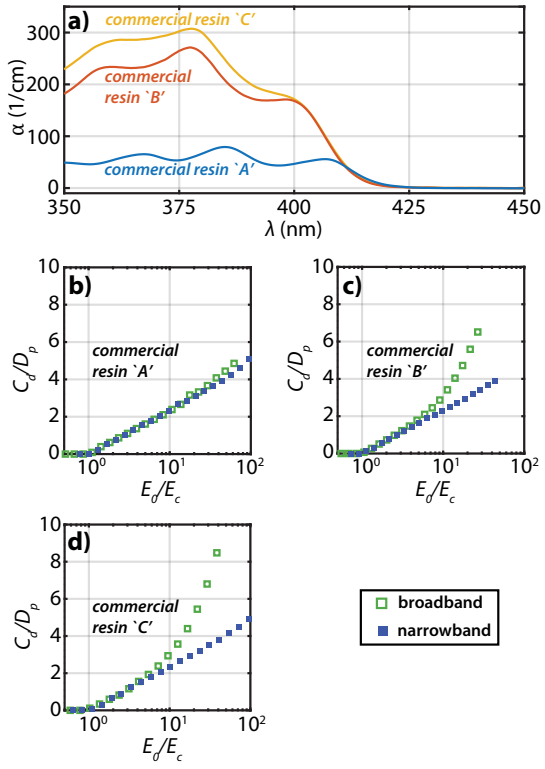

Figure 6: (a) The absorption coefficient for measured for three commercial 'clear' resins present in our laboratory. (b-d) Working curve data collected on these commercial resins using both narrowband and broadband illumination. Here, resin 'A' showed little variation between the two illumination schemes, while resins 'B' and 'C' show strong variation with the broadband data deviating strongly from the Jacobs model. All three of these resins appear optically identical to the eye. All working curves are plotted with a logarithmic exposure axis.

6. Discussion

As noted in the introduction, there are many reasons that a working curve may deviate from the Jacobs model. In certain resins, other phenomena (*e.g.* photobleaching) will be important to consider, however, for the resins studied here, the dominant effect was an inner filter effect whereby the spectrum of the light source is modified as it transmits through the resin. The data show that the polychromatic model accounts for the propagation of polychromatic light into the resin and is in nearly quantitative agreement with the experiment. This was tested in two separate ways. First, we showed that for a resin that deviates from the Jacobs model using broadband illumination, the working curve obtained using narrowband illumination was in good agreement with the Jacobs model. Second, we showed that for the same base resin system, modifying the photoblocker to flatten out the absorption over the light source bandwidth also brought the working curve data into good agreement with the Jacobs model.

Taken together, these experiments emphasize that the deviation from the Jacobs model will be the most notable when the optical properties of the resin vary significantly over the bandwidth of the light source. Modern LED sources tend to have relatively broadband spectra and so if the LED output is close to a gradient in the absorption spectrum of the resin then these effects will be evident. Such conditions are regularly present when curing 'clear' resins with a 405 nm LED light source. In contrast, 365 nm or 385 nm light sources are generally farther from any absorption gradients and may tend to evidence a less important inner filter effect (*e.g.* see Fig. 6a).

It is interesting to consider why photobleaching isn't more prevalent for the resins in this manuscript. To answer this we should first consider the absorption spectra in Fig. 3a. The photoinitiator, TPO, contributes $\leq 10\%$ to the total optical cross section of the resin and so even if the photoinitiator is completely consumed, then the overall absorption of the resin only changes modestly. Thus, a significant photobleaching effect would require the photoblocker to also photodegrade. Most photoblockers, however, are chosen specifically for their photostability[24]. And, in the context of photopolymerization, it is worth noting that diffusion is slow and oxygen is rapidly consumed[25, 26] such that the photostability of most dyes is likely increased during photopolymerization relative to ambient conditions. To be clear, however, there are certainly resins where photobleaching can dominate over polychromatic illumination effects. We would not wish the reader to assume that the polychromatic model is applicable to all systems. We only wish to point out that photobleaching should not be naively assumed when deviation from Jacobs model behavior is observed.

While the polychromatic model (Eq. 13) and the Jacobs model (Eq. 1) may appear quite distinct due to the more complex equations, we would like to emphasize that they are actually quite similar, conceptually. At least theoretically, E_c is the only free parameter in both models. In the Jacobs model, D_p is given by the resin absorption coefficient at the wavelength of the light source and fully specifies the model. In the polychromatic model, the model is fully specified by the absorption of the resin (and the photoinitator) in addition to the spectrum of the light source. In practice, however, these models differ based on how they can reasonably be used. Most of the time, the Jacobs model D_p is left as a free parameter and is never compared to the D_p that is taken from the absorption spectrum of the resin. In this case, the model is being used in an empirical fashion. Whereas, for the polychromatic model, there is no trivial single variable parameterization of the model that can be fit to the data that allows it to be used in a empirical fashion – instead, the optical properties of the system must be fully known to compute the model.

The preceding discussion also brings up another point that has been generally neglected in the literature. In the original derivation of the Jacobs model, the D_p parameter is presumed to be identical to the optical penetration depth of the resin as obtained through an absorption measurement[7]. In this case, the D_p is a well-defined optical parameter of the liquid resin. In contrast, determining a D_p by fitting the Jacobs model to working curve data yields a parameter D_p that, while likely being close to the optical D_p, wraps in many other phenomenon. For example, even neglecting all of the kinetics of photopolymerization, cure shrinkage alone would cause the fitted D_p to deviate from the optical D_p by several percent[27, 28]. Post-processing could possibly affect D_p, and the termination kinetics are also known to affect the fitted D_p. In this manuscript we have not used any notation to distinguish between the 'optical' D_p and the 'working curve' D_p, however, future studies should be cognizant of the difference and consider an improved nomenclature.

Finally, it is worth discussing this work in the context of the reproducibility of working curve measure-

ments. There are two separate points to consider. First, as noted in the derivation of the Jacobs model, the D_p and E_c parameters are fundamentally wavelength-dependent. And they are (very roughly) proportional to the inverse of the absorption coefficient. Thus, when a light source is centered near a strong gradient in the absorption of the resin, then the D_p and E_c parameters will be very sensitive to exact wavelength of the light source. Unfortunately, it is standard practice in the literature to cite the manufacturer's nominal wavelength instead of measuring the light source spectrum and the nominal wavelength can easily vary from the actual wavelength by up to 5 nm[29]. Therefore, whenever possible, it is important to obtain a direct measurement of the light source spectrum and/or state how the nominal wavelength was obtained.

Second, for resins that exhibit the inner filter effect discussed herein, the working curve exhibits significant curvature when plotted on a logarithmic exposure axis. In many studies, small cure depths are not measured due to a lack of available precision (< 5 µm) measuring devices. In these cases, the working curve data is obtained for a limited range of cure depths ($C_d >> D_p$) and fit to the Jacobs model, which (due to the curvature caused by polychromatic illumination) has a significant extrapolation error for both E_c and D_p. Depending on the exact range of data obtained and included in the fit, the D_p and E_c can vary significantly. Using the delta model may, in some circumstances, give a better fit and yield more reproducible parameters. We would suggest that, when possible, data should be obtained over a wide range of exposure and cure depth spaces. We believe that, in addition to plotting the raw data in the typical (E_0, C_d) coordinates, plotting working curve data in normalized coordinates $(E_0/E_c, C_d/D_p)$ can help to reveal potential extrapolation errors.

7. Conclusions

Herein we investigated the impact of an LED-based light source on working curve measurements. Experimentally we found that the relatively broad bandwidth of LED-based sources can lead to strong deviations from the Jacobs model for the working curve. Theoretically, we extended the Jacobs model for the working curve to account for polychromatic illumination and found agreement with experiment. In addition to a physics-based theoretical model, we presented the empirical delta model that is also able to better capture the functional form of working curves that do not conform to the original Jacobs model. This work serves to extend our understanding of the working curve measurement and provide improved working curve models to the VP community that will hopefully improve the reproducibility of these measurements.

Acknowledgments

We thank Karl Stupic for providing a sample of one of the commercial resins used herein. This work was performed while T.J.K. held a National Research Council Postdoctoral Associateship. We thank Brian Adzima for sharing an empirical working curve model functionally similar to the delta model presented in this manuscript. Finally, we would like to thank Paul F. Jacobs for constructive criticism of the manuscript.

Appendix A. Working Curve Fit Parameters

BBOT resin						
	broadband			narrowband		
	E_c (mJ/cm^2)	D_p (µm)	δ ($\times 10^3$)	E_c (mJ/cm^2)	D_p (µm)	δ ($\times 10^3$)
Jacobs model *(fit to data)*	29 ± 8	121 ± 18	-	6.1 ± 0.2	37 ± 1	-
delta model *(fit to data)*	11 ± 1	49 ± 2	24 ± 1	6.0 ± 0.3	37 ± 1	0
delta model *(fit to poly. model)*	-	42 ± 1	26 ± 1	-	41 ± 1	0

Sudan I resin						
	broadband			narrowband		
	E_c (mJ/cm^2)	D_p (µm)	δ ($\times 10^3$)	E_c (mJ/cm^2)	D_p (µm)	δ ($\times 10^3$)
Jacobs model *(fit to data)*	38 ± 2	63 ± 1	-	24 ± 1	62 ± 1	-
delta model *(fit to data)*	40 ± 1	67 ± 2	-3 ± 1	26 ± 1	66 ± 1	-2 ± 1
delta model *(fit to poly. model)*	-	72 ± 1	0	-	70 ± 1	0

commercial resins						
	broadband			narrowband		
	E_c (mJ/cm^2)	D_p (µm)	δ ($\times 10^3$)	E_c (mJ/cm^2)	D_p (µm)	δ ($\times 10^3$)
delta model *(fit to 'A' data)*	19 ± 1	224 ± 8	3 ± 1	13 ± 1	185 ± 6	1 ± 1
delta model *(fit to 'B' data)*	22 ± 1	77 ± 3	41 ± 2	14 ± 1	63 ± 2	1 ± 1
delta model *(fit to 'C' data)*	9.8 ± 0.6	114 ± 5	37 ± 2	5.3 ± 0.2	76 ± 2	1 ± 1

Table A.1: Fit parameters for the various experiments. Errors are given at the 95 % confidence interval for the least squares fit and do not include errors associated with replicate measurements or other systematic errors.

References

[1] H. Kodama, Automatic method for fabricating a three-dimensional plastic model with photo-hardening polymer, Rev. Sci. Instrum. 52 (11) (1981) 1770–1773. doi:10.1063/1.1136492.
URL http://aip.scitation.org/doi/10.1063/1.1136492

[2] C. W. Hull, Apparatus for Production of Three-Dimensonal Objects by Stereolithography (1986).

[3] S. M. Montgomery, C. M. Hamel, J. Skovran, H. J. Qi, A reaction–diffusion model for grayscale digital light processing 3D printing, Extrem. Mech. Lett. 53 (2022) 101714. doi:10.1016/j.eml.2022.101714.
URL https://linkinghub.elsevier.com/retrieve/pii/S2352431622000645

[4] S. Westbeek, J. Remmers, J. van Dommelen, H. Maalderink, M. Geers, Prediction of the deformed geometry of vat photo-polymerized components using a multi-physical modeling framework, Addit. Manuf. 40 (2021) 101922. doi:10.1016/j.addma.2021.101922.
URL https://linkinghub.elsevier.com/retrieve/pii/S2214860421000877

[5] K. Classens, T. Hafkamp, S. Westbeek, J. J. Remmers, S. Weiland, Multiphysical modeling and optimal control of material properties for photopolymerization processes, Addit. Manuf. 38 (2021) 101520. doi:10.1016/j.addma.2020.101520.
URL https://linkinghub.elsevier.com/retrieve/pii/S2214860420308927

[6] M. M. Emami, D. W. Rosen, Modeling of light field effect in deep vat polymerization for grayscale lithography application, Addit. Manuf. 36 (2020) 101595. doi:10.1016/j.addma.2020.101595.
URL https://linkinghub.elsevier.com/retrieve/pii/S2214860420309672
[7] P. F. Jacobs, Fundamentals of Stereolithography, in: Fundam. Stereolithography, 1992, p. 196.
[8] A. Thompson, B. N. Taylor, Guide for the Use of the International System of Units (SI), Tech. rep., National Institute of Standards and Technology, Gaithersburg, MD (2008).
URL http://physics.nist.gov/SP811
[9] H. Gong, B. P. Bickham, A. T. Woolley, G. P. Nordin, Custom 3D printer and resin for 18 μm $\times$ 20 μm microfluidic flow channels, Lab Chip 17 (17) (2017) 2899–2909. doi:10.1039/C7LC00644F.
URL http://xlink.rsc.org/?DOI=C7LC00644F
[10] J. Bennett, Measuring UV curing parameters of commercial photopolymers used in additive manufacturing, Addit. Manuf. 18 (2017) 203–212. doi:10.1016/j.addma.2017.10.009.
[11] D. A. Rau, J. P. Reynolds, J. S. Bryant, M. J. Bortner, C. B. Williams, A rheological approach for measuring cure depth of filled and unfilled photopolymers at additive manufacturing relevant length scales, Addit. Manuf. 60 (2022) 103207. doi:10.1016/j.addma.2022.103207.
URL https://linkinghub.elsevier.com/retrieve/pii/S2214860422005966
[12] Y. Rudenko, A. Lozovaya, L. Asanova, N. Fedyakova, P. Chapala, Light intensity influence on critical energy and penetration depth for vat photopolymerization technology, Prog. Addit. Manuf. (jun 2023). doi:10.1007/s40964-023-00474-z.
URL https://link.springer.com/10.1007/s40964-023-00474-z
[13] N. S. Kenning, D. Kriks, M. El-Maazawi, A. Scranton, Spatial and temporal evolution of the photoinitiation rate for thick polymer systems illuminated with polychromatic light, Polym. Int. 55 (9) (2006) 994–1006. doi:10.1002/pi.2047.
URL https://onlinelibrary.wiley.com/doi/10.1002/pi.2047
[14] N. S. Kenning, B. A. Ficek, C. C. Hoppe, A. B. Scranton, Spatial and temporal evolution of the photoinitiation rate for thick polymer systems illuminated by polychromatic light: selection of efficient photoinitiators for LED or mercury lamps, Polym. Int. 57 (10) (2008) 1134–1140. doi:10.1002/pi.2455.
URL https://onlinelibrary.wiley.com/doi/10.1002/pi.2455
[15] C. C. Hoppe, B. A. Ficek, H. S. Eom, A. B. Scranton, Cationic photopolymerization of epoxides containing carbon black nanoparticles, Polymer (Guildf). 51 (26) (2010) 6151–6160. doi:10.1016/j.polymer.2010.10.057.
URL https://linkinghub.elsevier.com/retrieve/pii/S0032386110009614
[16] W. F. Schroeder, S. L. Asmussen, W. D. Cook, C. I. Vallo, Efficiency of 4,4'-bis(N,N-diethylamino) benzophenone for the polymerization of dimethacrylate resins in thick sections, Polym. Int. (2011) n/a–n/adoi:10.1002/pi.3089.
URL https://onlinelibrary.wiley.com/doi/10.1002/pi.3089
[17] M. M. Emami, D. W. Rosen, An Improved Vat Photopolymerization Cure Model Demonstrates Photobleaching Effects, 2018 Int. Solid Free. Fabr. Symp. (2018). doi:10.26153/tsw/17195.
[18] L. M. Stevens, E. A. Recker, K. A. Zhou, V. G. Garcia, K. S. Mason, C. Tagnon, N. Abdelaziz, Z. A. Page, Counting All Photons: Efficient Optimization of Visible Light 3D Printing, Adv. Mater. Technol. (apr 2023). doi:10.1002/admt.202300052.
URL https://onlinelibrary.wiley.com/doi/10.1002/admt.202300052
[19] A. S. Jariwala, F. Ding, A. Boddapati, V. Breedveld, M. A. Grover, C. L. Henderson, D. W. Rosen, Modeling effects of oxygen inhibition in mask-based stereolithography, Rapid Prototyp. J. 17 (3) (2011) 168–175. doi:10.1108/13552541111124734.
URL https://www.emerald.com/insight/content/doi/10.1108/13552541111124734/full/html
[20] Y. Li, Q. Mao, J. Yin, Y. Wang, J. Fu, Y. Huang, Theoretical prediction and experimental validation of the digital light processing (DLP) working curve for photocurable materials, Addit. Manuf. 37 (2021) 101716. doi:10.1016/j.addma.2020.101716.
URL https://linkinghub.elsevier.com/retrieve/pii/S2214860420310885
[21] P. J. E. M. van der Linden, A. M. Popov, D. Pontoni, Accurate and rapid 3D printing of microfluidic devices using wavelength selection on a DLP printer, Lab Chip 20 (22) (2020) 4128–4140. doi:10.1039/D0LC00767F.
URL http://xlink.rsc.org/?DOI=D0LC00767F
[22] J. R. Lakowicz (Ed.), Principles of Fluorescence Spectroscopy, Springer US, Boston, MA, 2006. doi:10.1007/978-0-387-46312-4.
URL https://link.springer.com/10.1007/978-0-387-46312-4
[23] L. Feng, B. I. Suh, Exposure Reciprocity Law in Photopolymerization of Multi-Functional Acrylates and Methacrylates, Macromol. Chem. Phys. 208 (3) (2007) 295–306. doi:10.1002/macp.200600480.
URL https://onlinelibrary.wiley.com/doi/10.1002/macp.200600480
[24] M. A. Fourati, T. Maris, W. G. Skene, C. G. Bazuin, R. E. Prud'homme, Photophysical, Electrochemical and Crystallographic Investigations of the Fluorophore 2,5-Bis(5- tert -butyl-benzoxazol-2-yl)thiophene, J. Phys. Chem. B 115 (43) (2011) 12362–12369. doi:10.1021/jp207136k.
URL https://pubs.acs.org/doi/10.1021/jp207136k
[25] T. Scherzer, H. Langguth, Temperature Dependence of the Oxygen Solubility in Acrylates and its Effect on the Induction Period in UV Photopolymerization, Macromol. Chem. Phys. 206 (2) (2005) 240–245. doi:10.1002/macp.200400300.
URL https://onlinelibrary.wiley.com/doi/10.1002/macp.200400300
[26] A. K. O'Brien, C. N. Bowman, Modeling the Effect of Oxygen on Photopolymerization Kinetics, Macromol. Theory Simulations 15 (2) (2006) 176–182. doi:10.1002/mats.200500056.
URL https://onlinelibrary.wiley.com/doi/10.1002/mats.200500056

[27] K. Sekmen, T. Rehbein, M. Johlitz, A. Lion, A. Constantinescu, Thermal analysis and shrinkage characterization of the photopolymers for DLP additive manufacturing processes, Contin. Mech. Thermodyn. (aug 2022). doi:10.1007/s00161-022-01137-0.
URL https://link.springer.com/10.1007/s00161-022-01137-0

[28] K. Sekmen, T. Rehbein, M. Johlitz, A. Lion, A. Constantinescu, Curing-dependent thermo-viscoelastic and shrinkage behaviour of photopolymers, Mech. Mater. 179 (2023) 104566. doi:10.1016/j.mechmat.2023.104566.
URL https://linkinghub.elsevier.com/retrieve/pii/S0167663623000121

[29] B. W. Caplins, C. I. Higgins, T. J. Kolibaba, U. Arp, C. C. Miller, D. L. Poster, C. J. Zarobila, Y. Zong, J. P. Killgore, Characterizing light engine uniformity and its influence on liquid crystal display based vat photopolymerization printing, Addit. Manuf. 62 (2023) 103381. doi:10.1016/j.addma.2022.103381.
URL https://linkinghub.elsevier.com/retrieve/pii/S2214860422007709